J. Plasma Physics (2012), vol. 78, part 4, pp. 461–468. © Cambridge University Press 2012
doi:10.1017/S002237781200044X

Towards Sub-TeV electron beams driven by ultra-short, ultra-intense laser pulses

WEI-MIN WANG[1], ZHENG-MING SHENG[1,2], SHIGEO KAWATA[3], CHUN-YANG ZHENG[4], YU-TONG LI[1], LI-MING CHEN[1], QUAN-LI DONG[1], XIN LU[1], JING-LONG MA[1] and JIE ZHANG[1,2]

[1]Beijing National Laboratory of Condensed Matter Physics, Institute of Physics, CAS, Beijing 100190, China (hbwwm1@iphy.ac.cn)

[2]Key Laboratory for Laser Plasmas (Ministry of Education) and Department of Physics, Shanghai Jiao Tong University, Shanghai 200240, China

[3]Graduate School of Engineering, Utsunomiya University, 7-1-2 Yohtoh, Utsunomiya 321-8585, Japan

[4]Institute of Applied Physics and Computational Mathematics, Beijing 100094, China

(Received 31 October 2011; accepted 2 April 2012; first published online 4 May 2012)

Abstract. Energetic electron beam generation from a thin foil target by the ponderomotive force of an ultra-intense circularly polarized laser pulse is investigated. Two-dimensional particle-in-cell (PIC) simulations show that laser pulses with intensity of 10^{22}–10^{23} Wcm^{-2} generate about 1–10 GeV electron beams, in agreement with the prediction of one-dimensional theory. When the laser intensity is at 10^{24}–10^{25} Wcm^{-2}, the beam energy obtained from PIC simulations is lower than the values predicted by the theory. The radiation damping effect is considered, which is found to become important for the laser intensity higher than 10^{25} Wcm^{-2}. The effect of laser focus positions is also discussed.

1. Introduction

Laser wakefield accelerator (LWFA) has an acceleration field with strength of magnitude higher by three orders than the linear accelerator, and therefore LWFA can reduce the acceleration distance of electrons by three orders in principle. This provides the possibility to achieve a tabletop accelerator, which has broad applications in the generation of x-rays, γ-rays (DesRosiers et al. 2000; Glinec et al. 2005, 2006) and THz radiations (Leemans and Esarey 2003; Shen et al. 2007), as well as colliders physics (Gianotti and Quigg 2007; Leemans et al. 2009) etc. In the last decade, a great deal of progress has been made in LWFA (Pukhov and Meyer-ter- 2002; Faure et al. 2004, 2006; Geddes et al. 2004; Mangles et al. 2004; Leemans et al. 2006; Lu et al. 2006, 2007; Hafz et al. 2008; Wang et al. 2008a, b, 2009; Liu et al. 2011), in particular, 1-GeV monoenergetic electron beams were produced in about 1-cm distance plasmas (Leemans et al. 2006; Liu et al. 2011). At the same time, the ultra-short high-power laser technology has been developing fast. The next-generation laser pulse may have the intensity of up to 10^{25} Wcm^{-2} and a duration of few fs, e.g., the proposed Extreme Light Infrastructure (ELI). Such a laser pulse will provide new opportunities for particle acceleration. Meanwhile, it presents a parameter regime different from LWFA and therefore challenges LWFA. First, a very short laser pulse cannot efficiently excite the wakefield if its duration is much shorter than the plasma wavelength. Next, a too intense laser pulse will lead to the saturation of wakefield when the pulse can completely expel local electrons. On the other hand, such an ultra-short, ultra-intense laser pulse can drive laser ponderomotive force acceleration (LPFA) (Wang et al. 2010) very efficiently, since the ponderomotive force is proportional to laser intensity and inverse of laser duration. In this case, LPFA can have a higher acceleration field and can produce higher energy electron beams than LWFA (Lu et al. 2007; Wang et al. 2010). Furthermore, LPFA can be performed in vacuum. Hence, its acceleration field will not saturate if the laser intensity is lower than the threshold for vacuum polarization (Heisenberg and Euler 1936; Dittrich and Gies 2000).

In a recent work by Wang et al. (2010) a scheme for LPFA was proposed in which thin foil and thick foil targets were used. The thin foil target supplies the electron source of acceleration. The thick one reflects the laser pulse and allows an electron beam to go through when the beam is accelerated sufficiently. This scheme was demonstrated by two-dimensional (2D) particle-in-cell (PIC) simulations with the generation of a near 1-GeV electron beam with a laser pulse at 10^{22} Wcm^{-2}. In this paper, we investigate the electron energy scaling for a large range of laser intensity.

According to 1D theory (Yu et al. 2000; Meyer-ter-Vehn et al. 2001; Sheng et al. 2002; Wang et al. 2010), the

electron energy and the electron acceleration distance are linearly proportional to laser intensity, i.e., laser pulses at 10^{22}–10^{25} Wcm^{-2} can produce GeV–TeV electron beams a distance of 1 mm–1 m. Here we check this energy scaling by 2D PIC simulations. Effects of durations and spot sizes of lasers as well as transverse sizes of foil targets will also be discussed in detail. Since extremely intense laser pulses are employed, the electron radiation damping (RD) effect will be discussed by our 2D PIC code, including the RD process (Landau and Lifshitz 1975; Tamburini et al. 2010).

2. Scaling of electron energy in LPFA

We consider the motion of a test electron under the action of a plane, circularly polarized laser pulse. Assume that the laser pulse propagates along the $+x$ direction and its vector potential follows the form

$$\begin{aligned} A_y &= a_0 \sin(\pi\xi/\tau_0)\sin(2\pi\xi),\ 0 \leqslant \xi < \tau_0, \\ A_z &= a_0 \sin(\pi\xi/\tau_0)\cos(2\pi\xi),\ 0 \leqslant \xi < \tau_0, \end{aligned} \tag{2.1}$$

where $\xi = t - x$, t, and x are normalized by the laser period T and wavelength λ, τ_0 is the pulse duration, a_0 is normalized by $m_e c^2/e$, c is the speed of light in vacuum, and e and m_e are electron charge and rest mass, respectively. According to the Hamiltonian approach (Yu et al. 2000; Meyer-ter-Vehn et al. 2001; Sheng et al. 2002; Wang et al. 2010), one can obtain the electron momenta, $p_x = (A_y^2 + A_z^2)/2$, $p_y = A_y$, and $p_z = A_z$, the relativistic factor, $\gamma = (A_y^2 + A_z^2)/2 + 1$, and the ponderomotive force, $F_P = -\partial\gamma/\partial x$, where the momenta are normalized by $m_e c$. In terms of (2.1), one can easily give the relativistic factor as

$$\gamma = \frac{a_0^2}{2}\sin^2\left(\frac{\pi\xi}{\tau_0}\right) + 1, \tag{2.2}$$

and the ponderomotive force as

$$F_P = \frac{\pi a_0^2}{2\tau_0}\sin\left(\frac{2\pi\xi}{\tau_0}\right). \tag{2.3}$$

According to (2.3), the electron is at acceleration stage when $\xi \leqslant \tau_0/2$. Therefore, the acceleration distance of the electron is given by (Wang et al. 2010)

$$l_{\rm acc} = \frac{\tau_0 a_0^2}{8}. \tag{2.4}$$

At $\xi = \tau_0/2$ or $x = l_{\rm acc}$, the electron gains its maximum energy,

$$E_{\rm max} = 0.255\, a_0^2\ \text{MeV}. \tag{2.5}$$

If a 800-nm wavelength laser pulse with the peak intensity of I_0 is taken, (2.4) and (2.5) can be rewritten as

$$l_{\rm acc} = 0.23\frac{I_0}{10^{22}\ \text{Wcm}^{-2}}\ \frac{\tau_0}{T}\ \text{mm}, \tag{2.6}$$

and

$$E_{\rm max} = 0.6\frac{I_0}{10^{22}\ \text{Wcm}^{-2}}\ \text{GeV}. \tag{2.7}$$

In the following, we perform 2D PIC simulations to check the electron energy scaling presented above. A 800-nm wavelength laser pulse propagates along the $+x$ direction. Its vector potential takes the form of

$$\begin{aligned} A_y &= a_0 \sin(\pi\xi/\tau_0)\sin(2\pi\xi)\exp(-y^2/r^2),\ 0 \leqslant \xi < \tau_0, \\ A_z &= a_0 \sin(\pi\xi/\tau_0)\cos(2\pi\xi)\exp(-y^2/r^2),\ 0 \leqslant \xi < \tau_0. \end{aligned}$$

A foil target is taken as a plasma with the electron density of 0.2 n_c and the thickness of 1 μm, which is equivalent to the foil plasma with a density of 100 n_c and a thickness of 2 nm, where $n_c = 1.7 \times 10^{21}$ cm^{-3} is the critical density for the laser pulse of the 800 nm wavelength. Here we take the laser duration $\tau_0 = 2$ T, laser spot radius $r = 20\ \lambda$, and the foil transverse size as 2 λ. In the following subsections, we discuss the effects of the laser duration, spot radius, and the foil transverse size. It should be pointed out that we do not use the thick foil target to reflect laser pulse in this paper.

Figure 1 shows the spatial distributions of laser electric field as well as the number distributions of electrons as functions of energy and divergence angle. The laser intensity $I_0 = 1.7 \times 10^{22}$ Wcm^{-2} is taken. According to (2.6) and (2.7), the electron beam can be accelerated to 1-GeV energy at a distance of 0.78 mm. These are verified approximately by the results in Fig. 1. One can see that the electron beam is continuously accelerated. At 1.5 ps or at a distance of 0.45 mm, a monoenergetic beam is produced with the energy of around 0.8 GeV, the duration of about 1 fs, and a very small divergence angle. After this time the beam is decelerated, as shown in the plots at 3 ps. All of the electrons in the foil are pushed and accelerated, and therefore the charge of the beam is 0.14 n_c (assume that the size of the z-direction is also 2 λ).

Then we take $I_0 = 1.7 \times 10^{23}$ Wcm^{-2} and the simulation results are displayed in Fig. 2. One can see that the beam peak energy is up to 7 GeV at 5.5 ps or at a distance of 1.7 mm. The energy approaches the predicted value of 10 GeV from (2.7); however, the acceleration distance is much smaller than the predicted value of 7.8 mm from (2.6). The difference between the 1D theory and 2D simulations becomes even larger when the laser intensity is taken as 1.7×10^{24} Wcm^{-2}, with which the simulation results are plotted in Fig. 3. The energy of a monoenergetic beam reaches about 40 GeV at 40 ps or at a distance of 12 mm, while the predicted energy and acceleration distance are 100 GeV and 78 mm, respectively. The disagreements between the simulation results and the 1D theoretical ones can be attributed to mutidimensional effects of laser propagation and electron motion. From the spatial distributions of the laser field and electrons in Fig. 3, one can clearly observe the transverse motion of electrons, the de-focusing of the laser pulse, and the bending of the laser wavefront. These mutidimensional effects are not included in the 1D theory. The effects become stronger with increase of laser intensity.

https://doi.org/10.1017/S002237781200044X Published online by Cambridge University Press

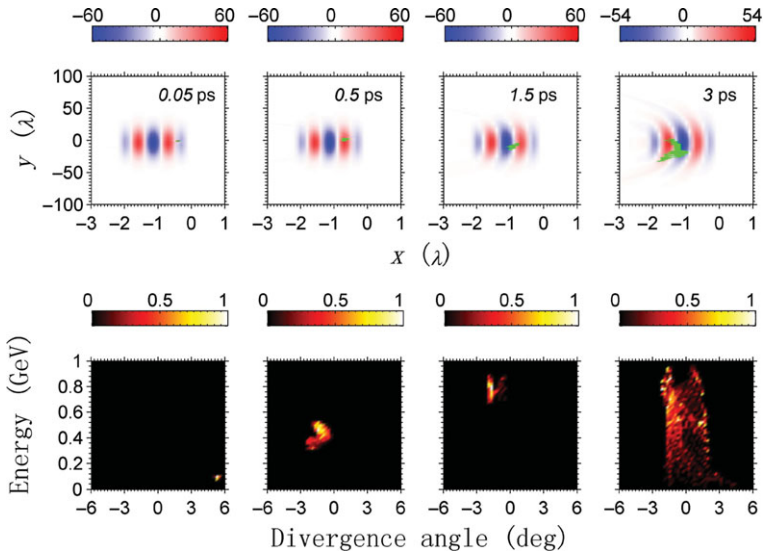

Figure 1. (Colour online) The upper row is snapshots of spatial distributions of the laser electric field E_y, where the green points denote electrons. The lower row is snapshots of number distributions of electrons as functions of energy and divergence angle. The laser intensity is 1.7×10^{22} Wcm^{-2}.

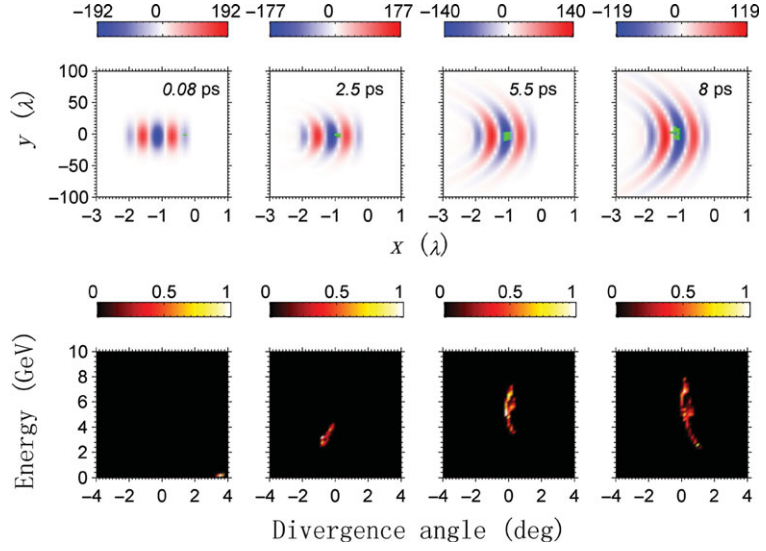

Figure 2. (Colour online) The upper row is snapshots of spatial distributions of the laser electric field E_y, where the green points denote electrons. The lower row is snapshots of number distributions of electrons as functions of energy and divergence angle. The laser intensity is 1.7×10^{23} Wcm^{-2}.

Figure 4 shows simulation results with the laser intensity of 1.7×10^{25} Wcm^{-2}. It is shown that the beam peak energy is up to 0.13 TeV at 64 ps or at a distance of 20 mm. Note that the corresponding values predicted from the 1D theory are 1 TeV and 780 mm. The results from Figs. 1–4 imply that ponderomotive force acceleration does not show saturation with the increasing laser intensity.

2.1. *Effect of the laser duration and spot size*

In this subsection, we discuss the impacts of laser durations, spot radii on electron acceleration. We take the laser durations as 2, 4, and 6 laser periods and the spot radii as 10, 20, and 30 laser wavelengths. The beam energies versus the laser durations and spot radii are shown in Fig. 5. One can see that beam energy basically decreases with increase of laser duration; for a very intense laser pulse (e.g. Figs. 5(c) and (d)), the beam energy with $r = 10\,\lambda$ is much lower than the ones with $r = 20\,\lambda$ and $30\,\lambda$. These can be explained as follows. At high laser intensity, the acceleration distance l_{acc} is larger than the Rayleigh distance $l_R = \pi r^2/\lambda = 0.25$ mm (Sun et al. 1987; Borisov et al. 1992; Wang and Zheng 2006) for $r = 10\,\lambda$. Thus, the laser pulse defocuses before the electrons are accelerated sufficiently. In addition, l_{acc} is larger than l_R even for a small laser duration with $\tau_0 = 2\ T$ and the difference between l_{acc} and l_R will be grown as the laser duration is increased to $\tau_0 = 4\ T$ and

https://doi.org/10.1017/S002237781200044X Published online by Cambridge University Press

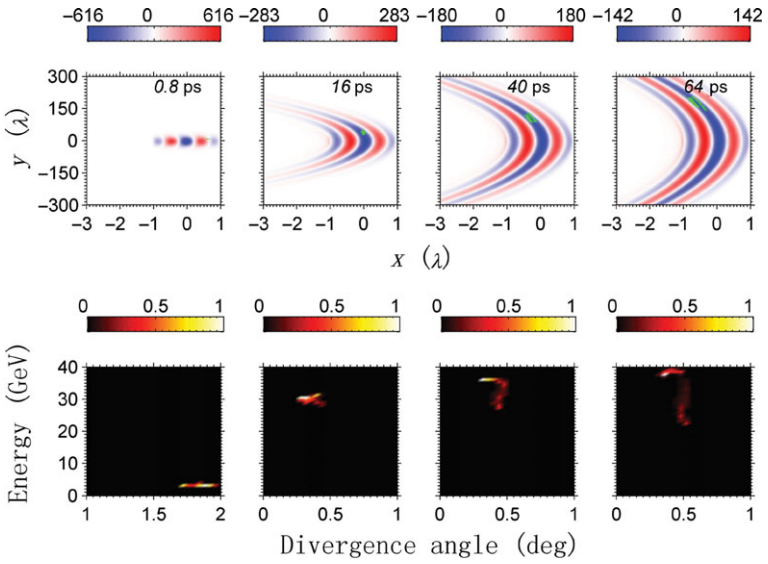

Figure 3. (Colour online) The upper row is snapshots of spatial distributions of the laser electric field E_y, where the green points denote electrons. The lower row is snapshots of number distributions of electrons as functions of energy and divergence angle. The laser intensity is 1.7×10^{24} Wcm^{-2}.

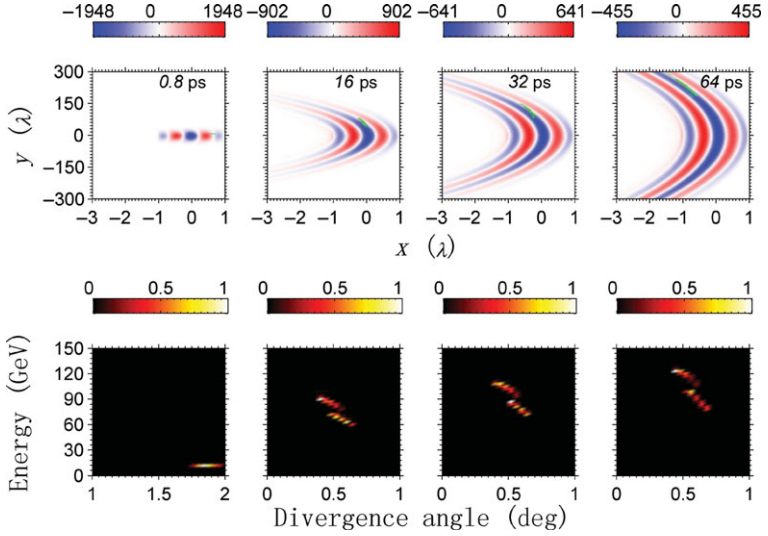

Figure 4. (Colour online) The upper row is snapshots of spatial distributions of the laser electric field E_y, where the green points denote electrons. The lower row is snapshots of number distributions of electrons as functions of energy and divergence angle. The laser intensity is 1.7×10^{25} Wcm^{-2}.

$\tau_0 = 6\,T$. Then electrons will experience more insufficient acceleration and therefore the beam energy decreases with increase in laser duration.

Besides, it is shown in Fig. 5 that the beam energy with $r = 30\,\lambda$ is not necessarily higher than the one with $r = 20\,\lambda$, which is resulted from complex coupling between the evolution of the laser pulse (e.g., the wavefront bending) and the transverse motion of electrons.

2.2. *Effect of the foil transverse size*

Then we discuss the effect of the foil transverse size on electron acceleration. In our simulations, the foil transverse sizes are taken within the range of 2–60 λ. It is found that with increase in the foil transverse size, the energy spread of the electron beam turns large. Two typical results are presented in Figs. 6 and 7 with the foil transverse sizes of 10 λ and 60 λ, respectively. Note that the latter is much larger than the laser spot radius of 20 λ. One can see in Fig. 6 that the beam still has a monoenergetic structure and an energy peak at about 40 GeV (the charge of the beam is $0.7\,n_c$). However, in Fig. 7 the ranges of energy spread and divergence angles of the beam electrons become broad. In this case the electrons diffuse in a broad space compared with Fig. 3 and therefore the energy spread is larger. As a result, to achieve a high quality electron beam it is necessary to take a foil with the transverse size smaller than the laser spot size.

https://doi.org/10.1017/S002237781200044X Published online by Cambridge University Press

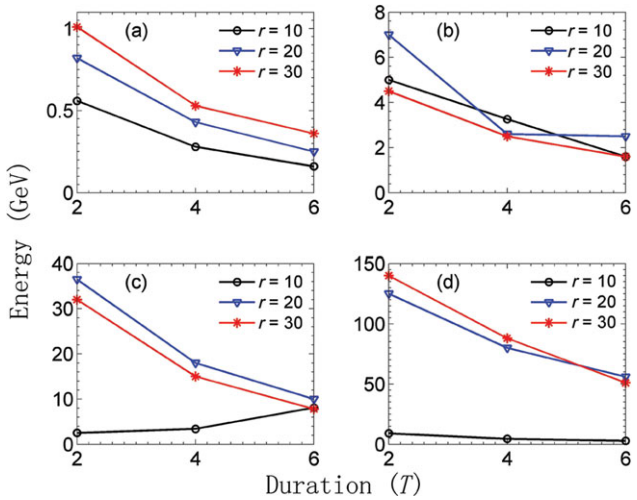

Figure 5. (Colour online) The beam peak energies as functions of laser durations τ_0 and spot radiuses r, where the laser intensities are taken as 1.7×10^{22}, 1.7×10^{23}, 1.7×10^{24}, and 1.7×10^{25} Wcm^{-2} in (a), (b), (c), and (d), respectively.

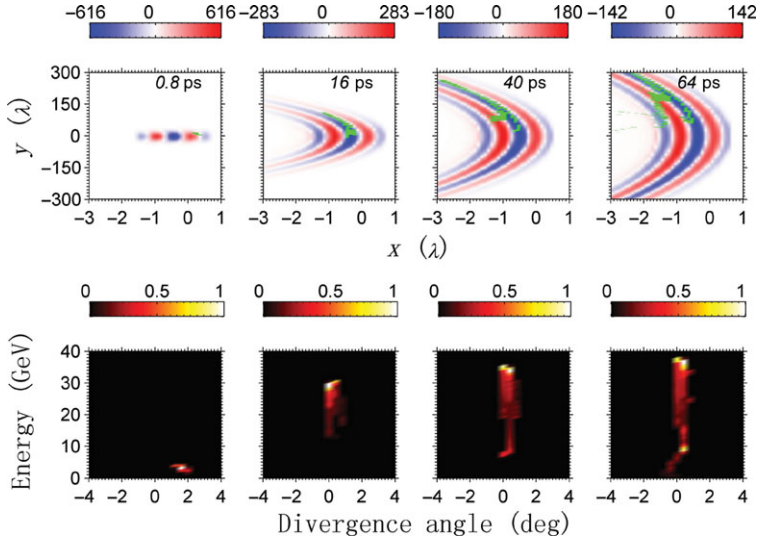

Figure 6. (Colour online) The upper row is snapshots of spatial distributions of the laser electric field E_y, where the green points denote electrons. The lower row is snapshots of number distributions of electrons as functions of energy and divergence angle. The foil transverse size is 10 λ and the laser parameters are same as in Fig. 3.

3. Effect of the radiation damping (RD)

We discuss the RD effect since an extremely intense laser pulse with the intensity of 10^{22}–10^{25} Wcm^{-2} has been used. We add the RD process to the PIC code through the algorithm proposed by Tamburini et al. (2010). It is shown in Fig. 8 that there is nearly no difference between the cases with and without RD. Hence, the RD effect does not need to be considered for LPFA with the laser intensity lower than 1.7×10^{24} Wcm^{-2}. When the laser intensity is grown to 1.7×10^{25} Wcm^{-2}, the difference between the cases with and without RD is still not large but can be observed in Fig. 9. The RD effect leads to some reduction in the maximum energy and the transverse momenta of electrons. Results in Figs. 8 and 9 indicate that when the laser intensity is of 10^{25} Wcm^{-2} order, the RD effect starts to become important for LPFA.

4. Effect of focus positions

In terms of (2.3), the peak of the acceleration field appears at $\xi = \tau_0/4$, at which electrons can be accelerated most efficiently. However, it requires an accelerating time period of $t_{acc}/2$ ($t_{acc} = l_{acc}/c$) for electrons to experience the peak acceleration field. Since the laser pulse experiences defocusing during propagation, the peak acceleration field will decrease. However, if the laser is focused at a distance away from the incident position, the laser field can increase at first before it propagates through the focus position. Then electrons

https://doi.org/10.1017/S002237781200044X Published online by Cambridge University Press

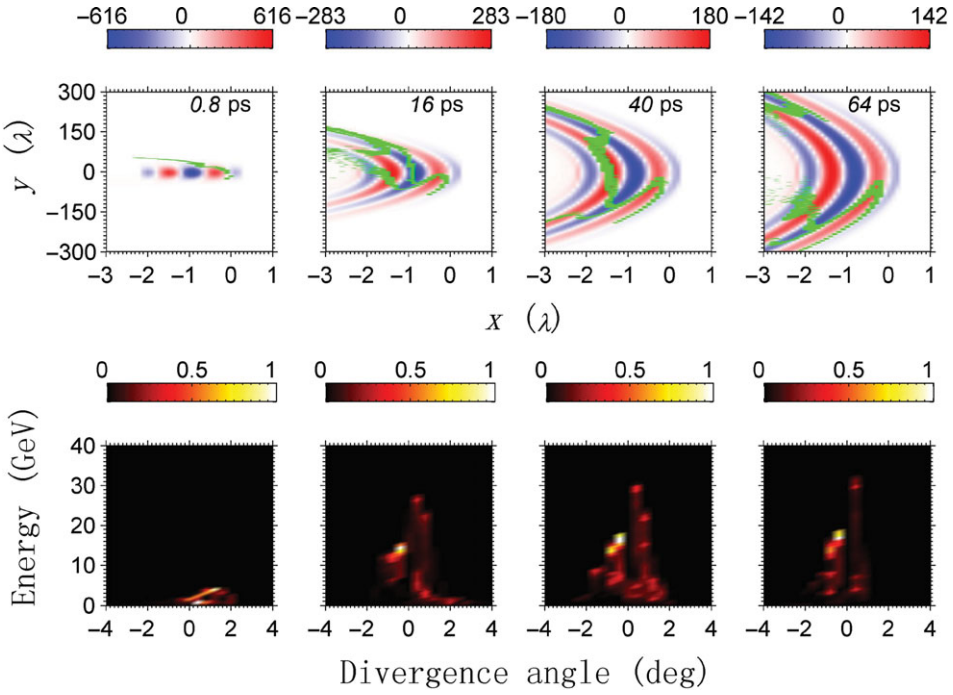

Figure 7. (Colour online) The upper row is snapshots of spatial distributions of the laser electric field E_y, where the green points denote electrons. The lower row is snapshots of number distributions of electrons as functions of energy and divergence angle. The foil transverse size is 60 λ and the laser parameters are the same as in Fig. 3.

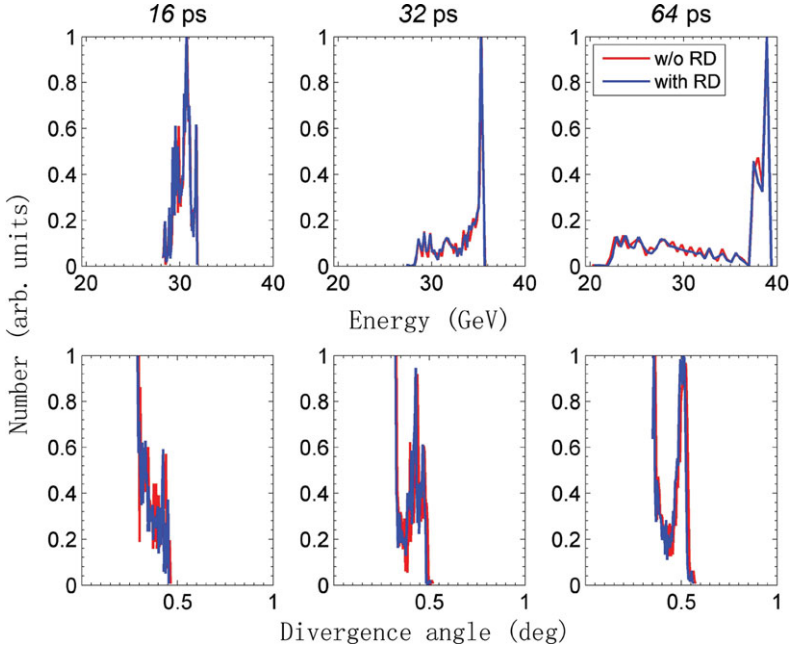

Figure 8. (Colour online) The upper row is the number distributions of electrons as a function of energy at different times. The lower row is the number distributions of electrons as a function of divergence angle at different times. The red curves denote simulations without the RD process and the blue ones with the RD process. The laser intensity is 1.7×10^{24} Wcm^{-2}.

may meet the peak acceleration field near the focus for more efficient acceleration. To examine this idea, we take the two sets of PIC simulations. In one set of simulations the laser intensity is fixed at 1.7×10^{22} Wcm^{-2} and the laser focus is taken at distances of 0.2–1.0 mm away from the incident position. In the other, the laser intensity is fixed at 1.7×10^{23} Wcm^{-2}. In the first set of simulations, the effect of focus positions is not obvious. In the second set of simulations, the effect of focus positions is appreciable, as observed in Fig. 10. The optimum focus position appears to be at 0.6 mm, with which the energy peak of the beam approaches to about 8.0 GeV and the

https://doi.org/10.1017/S002237781200044X Published online by Cambridge University Press

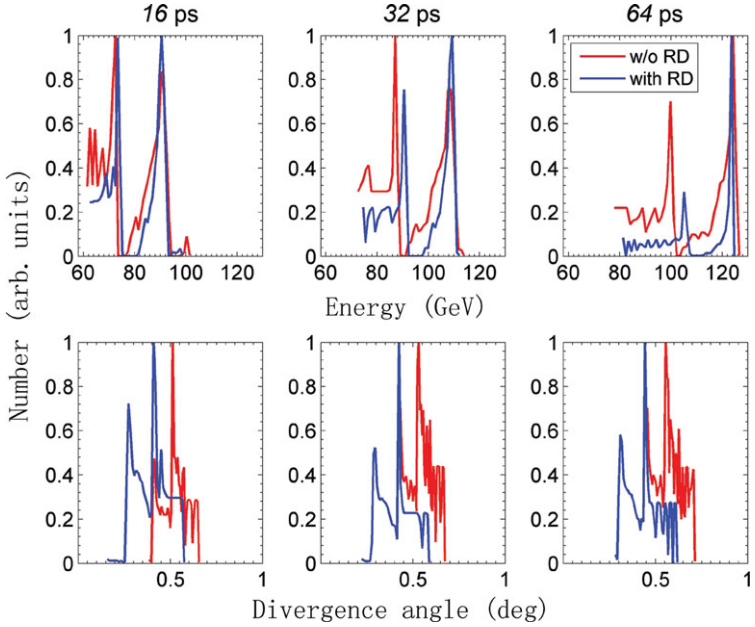

Figure 9. (Colour online) The upper row is the number distributions of electrons as a function of energy at different times. The lower row is the number distributions of electrons as a function of the divergence angle at different times. The red curves denote simulations without the RD process and the blue ones with the RD process. The laser intensity is 1.7×10^{25} Wcm^{-2}.

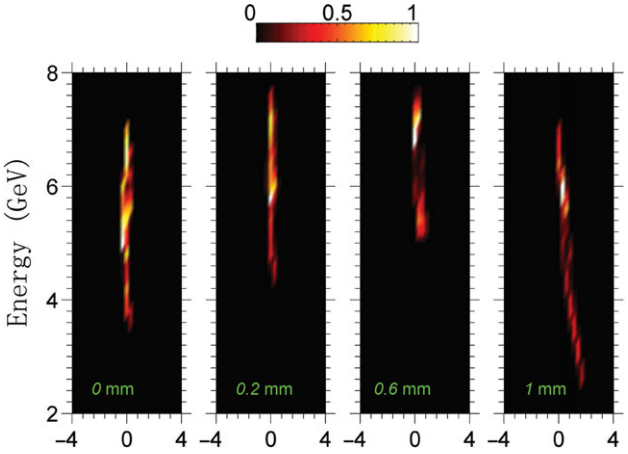

Figure 10. (Colour online) Number distributions of electrons as functions of the energy and divergence angle at 5.5 ps, where the laser focus positions are controlled at 0, 0.2, 0.6, and 1 mm away from the incident position of the laser pulse. The laser intensity is fixed at 1.7×10^{23} Wcm^{-2}.

energy spread is the smallest. The value of 0.6 mm is close to half of the actual acceleration distance (1.7 mm) seen in Fig. 2.

5. Summary

In summary, we have demonstrated by PIC simulations that GeV-TeV ultra-short monoenergetic electron beams can be generated through LPFA. For the laser intensities of $10^{22} - 10^{23}$ Wcm^{-2}, the beams are accelerated to energies of about 1-10 GeV, which is in agreement with the scaling given by the 1D theory. With the increase of laser intensities, the beam energies are below the scaling, e.g., the laser pulse at 10^{25} Wcm^{-2} produces 0.13 TeV electron beams while the predicted energy is 1 TeV. The deviation of beam energies obtained from simulations from the 1D theory is attributed to muti-dimensional effects of the laser propagation and the transverse motion of electrons. Besides, to obtain a monoenergetic beam, the transverse size of the foil target should be smaller than the laser spot size. It is also shown that for LPFA the RD effect should be considered when the laser intensity is higher than 10^{25} Wcm^{-2}. In addition, when the laser focus is taken at a distance at the order of half l_{acc} away from the incident position, the energy and quality of the beam can be enhanced.

Acknowledgements

This work is supported in part by the NSFC (Grants 11105217, 11121504 and 10925421), the National Basic Research Program of China (Grants 2009GB105002),

https://doi.org/10.1017/S002237781200044X Published online by Cambridge University Press

the JSPS and MEXT in Japan, and the CORE (Center for Optical Research and Education) program in Utsunomiya University, Japan.

References

Borisov, A. B. et al. 1992 *Phys. Rev.* A **45**, 5830.

DesRosiers, C., Moskvin, V., Bielajew, A. F. and Papiez, L. 2000 *Phys. Med. Biol.* **45**, 1781.

Dittrich, W. and Gies, H. 2000 *Probing the Quantum Vacuum.* Berlin, Germany: Springer-Verlag.

Faure, J. et al. 2004 *Nature* (London) **431**, 541.

Faure, J. et al. 2006 *Nature* (London) **444**, 737.

Geddes, C. et al. 2004 *Nature* (London) **431**, 538.

Gianotti, F. and Quigg, F. C. 2007 Phys. Today, September, 90.

Glinec, Y., Faure, J., Malka, V., Fuchs, T., Szymanowski, H. and Oelfke, U. 2006 *Med. Phys.* **33**, 155.

Glinec, Y. et al. 2005 *Phys. Rev. Lett.* **94**, 025003.

Hafz, N. A. M. et al. 2008 *Nature Photonics* **2**, 571.

Heisenberg, W. and Euler, H. 1936 *Z. Phys.* **98**, 714.

Landau, L. D. and Lifshitz, E. M. 1975 *The Classical Theory of Fields*, Chap. 76, 2nd edn. Oxford, UK: Elsevier.

Leemans, W. P. and Esarey, E. 2009 *Phys.* Today, March, 44.

Leemans, W. P. et al. 2003 *Phys. Rev. Lett.* **91**, 074802.

Leemans, W. P. et al. 2006 *Nature Phys.* **2**, 696.

Liu, J. S. et al. 2011 *Phys. Rev. Lett.* **107**, 035001.

Lu, W. et al. 2006 *Phys. Rev. Lett.* **96**, 165002.

Lu, W. et al. 2007 *Phys. Rev. ST Accel. Beams* **10**, 061301.

Mangles, S. P. D. et al. 2004 *Nature* (London) **431**, 535.

Meyer-ter-Vehn, J., Pukhov, A. and Sheng, Z.-M. 2001 In: *Atoms, Solids, and Plasmas in Super-Intense Laser Fields* (ed. D. Batani et al.). Dordrecht, Netherlands: Kluwer, pp. 167–192.

Pukhov, A. and Meyer-ter-vehn, J. 2002 *Appl. Phys.* B **74**, 355.

Shen, Y., Watanabe, T., Arena, D. A., Kao, C.-C., Murphy, J. B., Tsang, T. Y., Wang, X. J. and Carr, G. L. 2007 *Phys. Rev. Lett.* **99**, 043901.

Sheng, Z.-M. et al. 2002 *Phys. Rev. Lett.* **88**, 055004.

Sun, G.-Z. et al. 1987 *Phys. Fluids* **30**, 526.

Tamburini, M. et al. 2010 *New J. Phys.* **12** ,123005.

Wang, W.-M. and Zheng, C.-Y. 2006 *Phys. Plasmas* **13**, 053112.

Wang, W.-M. et al. 2008a *Appl. Phys. Lett.* **93**, 201502.

Wang, W.-M. et al. 2008b *Phys. Plasmas* **15**, 013101.

Wang, W.-M. et al. 2009 *Laser Part. Beams* **27**, 3.

Wang, W.-M. et al. 2010 *Phys. Rev. ST Accel. Beams* **13**, 071301.

Yu, W. et al. 2000 *Phys. Rev. Lett.* **85**, 570.